Academy Transaction Note "Two-Stage Automatic Mass Balancing and Attitude Control for 3-DoF Spacecraft Attitude Simulators"

Yong-Hwan Kim[a,*], Kyungryeung Min[a], Yangchan Cho[a,*]

[a] *Space n Bean Inc., 232 Gongneung-ro, Nowon-gu, Seoul, 01811, Republic of Korea*

Abstract

Two-stage automatic mass balancing is experimentally demonstrated on a hemispherical 3-DoF spacecraft attitude simulator. CRAMBO performs coarse offset reduction, while FRAMBO refines the dynamic-equivalent CR-CG estimate to approximately $[0.08, 0.12, -27.62]$ μm. The final estimate is used for gravity-torque feedforward during a coupled three-axis hardware maneuver with sub-degree attitude tracking.

Keywords: 3-DoF air-bearing simulator, spacecraft attitude simulator, automatic mass balancing, CR-CG offset estimation, batch least-squares estimation

1. Introduction

Three-degree-of-freedom (3-DoF) air-bearing simulators provide a nearly frictionless environment for ground-based hardware-in-the-loop validation of spacecraft attitude determination and control systems (ADCS) [1–3]. Their performance is strongly affected by the offset between the center of rotation (CR) and center of gravity (CG), which generates gravity-induced torque in a 1-g environment [4–6].

Automatic mass balancing using movable masses and CR-CG estimation has therefore been investigated [5–8]. Practical implementation, however, is affected by non-orthogonal slider axes, actuator resolution and repeatability, sensor uncertainty, and unmodeled disturbances [3, 9, 10]. For the present hemispherical platform, a slightly negative vertical CR-CG offset is retained to preserve pendulum-like passive stability [4].

This study experimentally demonstrates the Robust Automatic Mass Balancing Operator (RAMBO), a two-stage framework combining coarse balancing (CRAMBO) and fine balancing (FRAMBO) with batch least-squares CR-CG estimation and sequential estimate-and-correct operation. FRAMBO additionally uses stop-and-restart reinitialization to refine the residual dynamic-equivalent CR-CG offset. The final estimate is then used as a fixed parameter for gravity-torque feedforward in a conventional quaternion proportional-derivative controller, and the complete hardware sequence is validated through three-axis attitude and angular-velocity responses.

2. System Configuration and Methods

2.1. Simulator Configuration and Dynamics

The experimental platform is a hemispherical air-bearing 3-DoF spacecraft attitude simulator with unrestricted yaw and mechanically limited roll/pitch of ±30°. It integrates sensing, reaction-wheel actuation, automatic mass balancing, and onboard processing on a single floating platform, as shown in Fig. 1. The principal hardware components and specifications are summarized in Table 1.

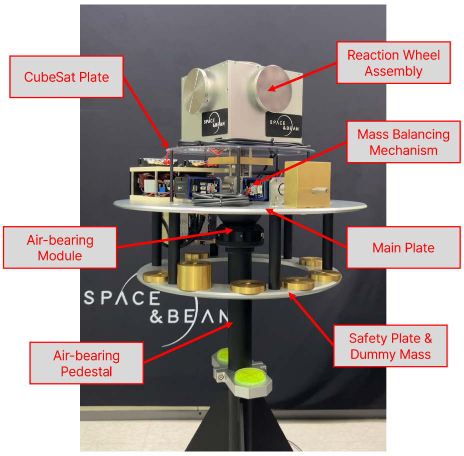

Figure 1: Overall mechanical configuration of the 3-DoF simulator.

A VectorNAV VN-100 IMU/AHRS provides primary attitude and angular-rate measurements, while a WITMotion BWT901CL provides secondary roll/pitch checks. Three reaction-wheel assemblies generate control torques, three independently actuated sliding masses adjust the platform CG, and a Raspberry Pi 5 executes RAMBO, attitude control, actuator commands, and data logging.

The inertial and body-fixed frames are denoted by $\mathcal{F}_N$ and $\mathcal{F}_B$, with the origin of $\mathcal{F}_B$ at the air-bearing center of rotation (CR). The CR-CG offset and slider displacement are defined as $\mathbf{r}_{cg} = [x_{cg}\ y_{cg}\ z_{cg}]^T$ and $\mathbf{s} = [s_x\ s_y\ s_z]^T$, respectively. Figure 2 shows the coordinate definitions and sliding-mass geometry.

For an incremental slider displacement,

*Corresponding authors.
Email addresses: kyh@spacenbean.com (Yong-Hwan Kim), silence.cho@spacenbean.com (Yangchan Cho)

Table 1: Main hardware components and specifications of the 3-DoF spacecraft attitude simulator.

Component	**Manufacturer / Model**	**Key specification**
Hemispherical air bearing	Physik Instrumente / A-653.045	Sphere diameter: 100 mm
Floating platform	In-house	m_{tot} = 26.95 kg; J_{xx}, J_{yy}, J_{zz} = 0.612, 0.684, 0.668 kg·m^2
Primary IMU/AHRS	VectorNAV / VN-100	attitude and angular-rate feedback
Secondary IMU	WITMotion / BWT901CL	roll/pitch consistency check
Reaction wheel assembly	Maxon EC-45 flat / EPOS Compact 50/5 / ENC MILE / in-house wheel disk	Rated speed: 3000 RPM; maximum torque: 48.6 mN·m; angular momentum: 97.2 mN·m·s
Sliding-mass actuator	Leadshine / iCS-RS1706	Positioning resolution: 5.0 µm
Sliding masses	In-house	m_x, m_y, m_z = 1.5, 1.5, 1.0 kg; stroke: ±32.5 mm (x/y), ±23.0 mm (z)
Control computer	Raspberry Pi 5	RAMBO, attitude control, actuator commands, and data logging

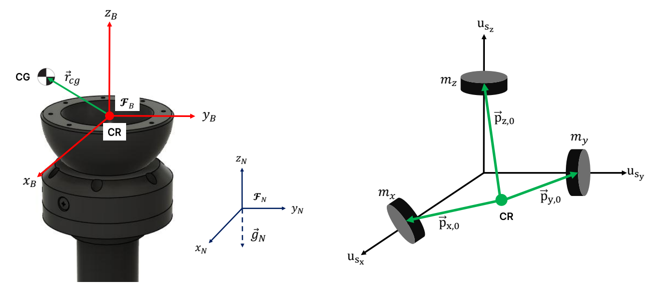

(a) Coordinate-frame definition. (b) Sliding-mass geometry.

Figure 2: Mass-balancing configuration: (**a**) coordinate-frame and CR-CG offset definition; (**b**) sliding-mass geometry.

$$\Delta \mathbf{r}_{cg} = \frac{1}{m_{\mathrm{tot}}} \mathbf{U}_s \mathbf{M}_s \Delta \mathbf{s}, \tag{1}$$

where $\mathbf{U}_s = [\hat{\mathbf{u}}_{s_x}\ \hat{\mathbf{u}}_{s_y}\ \hat{\mathbf{u}}_{s_z}]$ contains the slider-axis unit vectors and $\mathbf{M}_s = \mathrm{diag}(m_x, m_y, m_z)$. Ideally, $\mathbf{U}_s = \mathbf{I}$; slight installation non-orthogonality causes cross-axis coupling, which is handled by the iterative balancing procedure in Section 2.2.

In a 1-g environment, a residual CR-CG offset generates the attitude-dependent gravity torque

$$\boldsymbol{\tau}_g = \mathbf{r}_{cg}^{\times} (m_{\mathrm{tot}} \mathbf{g}_B), \qquad \mathbf{g}_B = \mathbf{C}_{BN} [0\ 0\ -g]^T. \tag{2}$$

A slightly negative z_{cg} is retained for passive restoring stability. Modeling the floating platform as a rigid body about the air-bearing CR gives

$$\mathbf{J}\dot{\boldsymbol{\omega}} + \boldsymbol{\omega}^{\times}\mathbf{J}\boldsymbol{\omega} = \boldsymbol{\tau}_c + \boldsymbol{\tau}_g + \boldsymbol{\tau}_d, \tag{3}$$

where $\mathbf{J}$ is the CAD-estimated inertia matrix, $\boldsymbol{\omega}$ is the body angular velocity, and $\boldsymbol{\tau}_c$ and $\boldsymbol{\tau}_d$ denote the control torque and unmodeled disturbances, respectively.

2.2. CR-CG Estimation and Two-Stage Balancing

RAMBO comprises a coarse stage (CRAMBO) followed by a fine stage (FRAMBO), both using free-response measurements and batch least-squares (BLS) CR-CG offset estimation based on [11, 12]. During each estimation window, reaction-wheel control is disabled. Under a simplified gravity-dominated free-response model,

$$\Delta \boldsymbol{\omega}_k = \boldsymbol{\Phi}_k \mathbf{r}_{cg}, \qquad \Delta \boldsymbol{\Omega}_L = \boldsymbol{\Phi}_L \mathbf{r}_{cg}, \tag{4}$$

where $\Delta\boldsymbol{\omega}_k = \boldsymbol{\omega}_{k+1} - \boldsymbol{\omega}_k$, and $\Delta\boldsymbol{\Omega}_L$ and $\boldsymbol{\Phi}_L$ are formed by stacking N sampling intervals. For full-column-rank $\boldsymbol{\Phi}_L$, the BLS estimate is

$$\hat{\mathbf{r}}_{cg} = \left(\boldsymbol{\Phi}_L^T \boldsymbol{\Phi}_L\right)^{-1} \boldsymbol{\Phi}_L^T \Delta\boldsymbol{\Omega}_L. \tag{5}$$

The estimate is interpreted as a dynamic-equivalent CR-CG offset that may include sensor errors, unmodeled disturbances, and modeling approximations. The nominal slider correction is

$$\Delta s_{\mathrm{raw},i} = \left(\hat{r}_{cg,\mathrm{tar},i} - \hat{r}_{cg,i}\right) \frac{m_{\mathrm{tot}}}{m_i}, \qquad i \in \{x, y, z\}. \tag{6}$$

For each stage, the estimate is evaluated against stage-specific lateral and vertical admissible conditions,

$$|\hat{x}_{cg}|, |\hat{y}_{cg}| \le \alpha_j, \qquad \beta_{j,l} \le \hat{z}_{cg} \le \beta_{j,u}, \qquad j \in \{C, F\}, \tag{7}$$

where C and F denote CRAMBO and FRAMBO, respectively. The corresponding bounds, estimation windows, and weighting factors are given in Table 2.

CRAMBO applies stage-weighted slider corrections and automatically repeats the estimate-and-correct cycle until the coarse admissible conditions are satisfied, providing the initial balanced state for FRAMBO [Fig. 3(a)]. FRAMBO then applies smaller, condition-dependent corrections within tighter bounds. Each FRAMBO trial terminates after one estimate-and-correct operation, followed by stop-and-restart reinitialization before the next trial [Fig. 3(b)]. The final $\hat{\mathbf{r}}_{cg}$ satisfying the fine admissible conditions is retained for subsequent attitude-control testing.

2.3. Hardware Attitude Control

Following RAMBO, the final FRAMBO estimate, $\hat{\mathbf{r}}_{cg}$, is retained as a fixed parameter for hardware attitude control. A conventional quaternion PD controller is used [13, 14], with $\mathbf{q}_e = (\mathbf{q}_t^{-1})^{\otimes}\mathbf{q}_s$, $q_{e,4} \ge 0$, and $\boldsymbol{\omega}_e = \boldsymbol{\omega}_c - \boldsymbol{\omega}$, where $\boldsymbol{\omega}_c = \mathbf{0}$.

Using the FRAMBO estimate for gravity-torque feedforward [15], the commanded platform torque is

$$\boldsymbol{\tau}_c = -\mathbf{K}_p \mathbf{q}_{e,v} - \mathbf{K}_d \boldsymbol{\omega}_e - \hat{\mathbf{r}}_{cg}^{\times} (m_{\mathrm{tot}} \mathbf{g}_B). \tag{8}$$

During the maneuver, $\hat{\mathbf{r}}_{cg}$ is fixed while $\mathbf{g}_B$ is updated from the measured attitude. Since the three reaction wheels are aligned with the body axes, $\boldsymbol{\tau}_{rw,cmd} = -\boldsymbol{\tau}_c$ without redundant control allocation. Controller parameters and test conditions are given in Table 3.

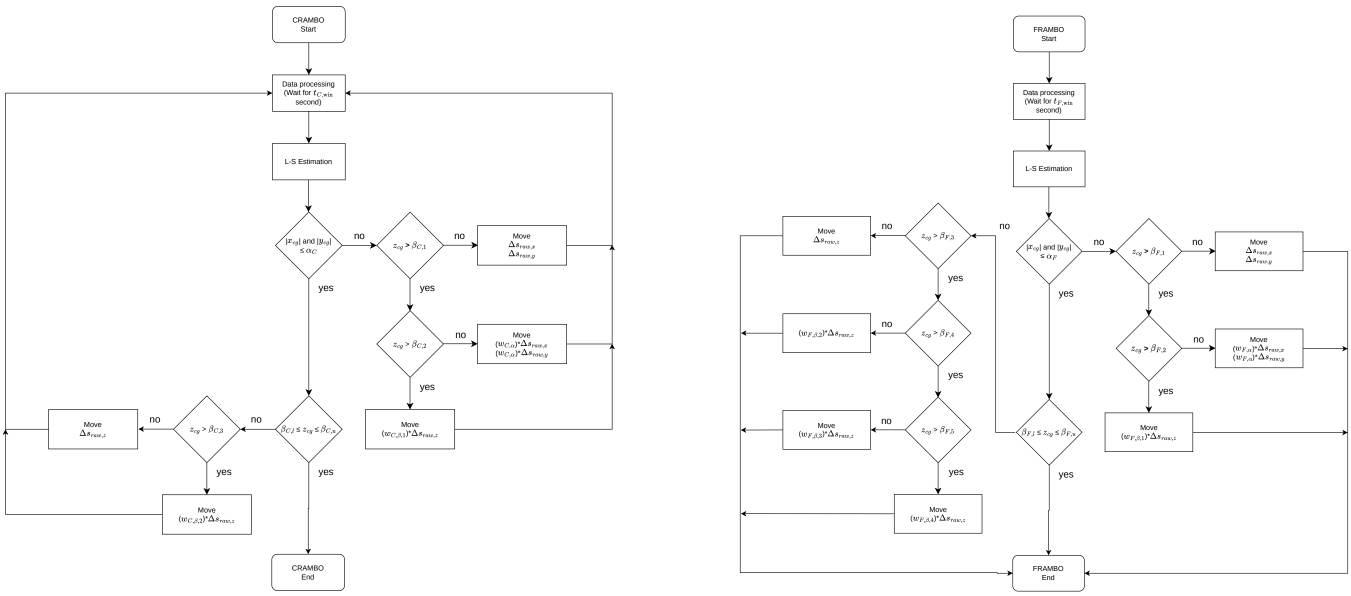

(a) CRAMBO.

(b) FRAMBO.

Figure 3: Operational flowcharts of the two-stage RAMBO procedure: (**a**) CRAMBO; (**b**) FRAMBO.

3. Experimental Validation

Hardware validation comprised RAMBO-based mass balancing followed by a coupled three-axis attitude-control test. The balancing parameters are summarized in Table 2, and the attitude-control requirements, controller gains, and test conditions are given in Table 3.

Table 2: RAMBO admissible conditions and experimental parameters.

Parameter	**CRAMBO**	**FRAMBO**
Lateral admissible condition	$\lvert\hat{x}_{cg}\rvert, \lvert\hat{y}_{cg}\rvert < 1$ μm	$\lvert\hat{x}_{cg}\rvert, \lvert\hat{y}_{cg}\rvert < 0.5$ μm
Vertical admissible range	$-100 < \hat{z}_{cg} < -70$ μm	$-30 < \hat{z}_{cg} < -20$ μm
Target vertical offset	−75 μm	−25 μm
Estimation window, t_{win}	40 s	80 s
Lateral weighting, w_α	0.5	0.5
Vertical weighting, $w_{\beta,k}$	0.6, 0.6	0.3, 0.6, 0.3, 0.3

Table 3: Attitude-control test conditions and controller parameters.

Category	**Parameter**	**Value**
Requirement	Attitude error	$< 1°$
	Angular velocity error	$< 0.5°$/s
Control	IMU sampling rate	50 Hz
	RW communication rate	5 Hz
	RW speed-command interval	1.0 s
	Proportional gain, $\mathbf{K}_p$	diag([0.27, 0.28, 0.10]) N·m
	Derivative gain, $\mathbf{K}_d$	diag([1.00, 1.04, 0.36]) N·m·s
Test case	Initial attitude	$[0, 0, 0]^T$ deg
	Target attitude	$[15, -10, 35]^T$ deg
	Target angular velocity	$[0, 0, 0]^T$ deg/s
Deadband	Attitude error	0.3°
	Angular velocity error	0.3°/s

3.1. Mass-Balancing Validation

Before CRAMBO, the platform was manually pre-balanced to prevent excessive initial tipping. CRAMBO reduced the estimated CR-CG offset from $[1.562,\ 1.810,\ -265.142]^T$ μm to $[0.303,\ 0.005,\ -95.083]^T$ μm over eight iterations. FRAMBO subsequently refined the offset over eleven stop-and-restart trials to $[0.083,\ 0.115,\ -27.621]^T$ μm.

Figure 4 shows the CR-CG offset convergence through both stages, with FRAMBO refining the residual offset into the fine admissible range.

Tables 4 and 5 provide the detailed balancing records, where $\Delta s_{\text{raw},i}$ and $\Delta s_{\text{cmd},i}$ denote the pre-weighting correction and applied slider command, respectively, and enc_i is the accumulated encoder position.

No additional slider commands were applied in the final two FRAMBO trials, and both estimates remained within the fine admissible range, supporting the final value as the dynamic-equivalent CR-CG estimate used for attitude-control testing.

3.2. Hardware Attitude-Control Validation

Following RAMBO, the testbed executed a coupled three-axis maneuver from $(0°, 0°, 0°)$ to $(15°, -10°, 35°)$ using the final FRAMBO estimate for gravity-torque feedforward.

Figure 5 shows the measured attitude and angular-velocity responses and tracking errors. The VN-100 estimates show attitude errors within approximately ±0.5° and angular-velocity errors within ±0.4°/s for roll and ±0.2°/s for pitch and yaw. WITMotion measurements are included only for secondary roll/pitch consistency; yaw was excluded because of magnetic-field distortion.

The measured attitude and angular-velocity responses demonstrate three-axis hardware attitude control in the

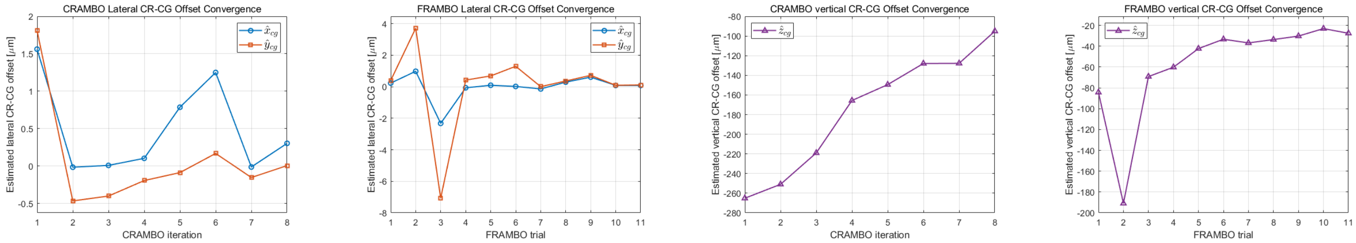

(a) CRAMBO lateral. (b) FRAMBO lateral. (c) CRAMBO vertical. (d) FRAMBO vertical.

Figure 4: Estimated CR-CG offset convergence during RAMBO: (**a**) CRAMBO lateral components; (**b**) FRAMBO lateral components; (**c**) CRAMBO vertical component; (**d**) FRAMBO vertical component.

Table 4: Detailed CRAMBO balancing records. The estimated CR-CG offsets are given in µm, and the slider commands and encoder positions are given in degrees.

Iter.	$\hat{x}_{cg}$ [µm]	$\hat{y}_{cg}$ [µm]	$\hat{z}_{cg}$ [µm]	$\Delta s_{\text{raw},x}$ [deg]	$\Delta s_{\text{raw},y}$ [deg]	$\Delta s_{\text{raw},z}$ [deg]	$\Delta s_{\text{cmd},x}$ [deg]	$\Delta s_{\text{cmd},y}$ [deg]	$\Delta s_{\text{cmd},z}$ [deg]	enc_x [deg]	enc_y [deg]	enc_z [deg]
1	1.5615	1.8100	-265.142	-10.2207	-11.8470	1806.0982	10.2207	11.8470	0	10.044	11.628	0
2	-0.0156	-0.4661	-250.971	0.1020	3.0507	1671.4923	0	0	-360	10.044	11.628	-359.856
3	0.0088	-0.4010	-219.011	-0.0574	2.6250	1367.9145	0	0	-360	10.044	11.628	-719.856
4	0.1030	-0.1940	-165.652	-0.6745	1.2699	861.0744	0	0	-360	10.044	11.628	-1079.86
5	0.7859	-0.0877	-149.482	-5.1442	0.5739	707.4807	0	0	-360	10.044	11.628	-1439.82
6	1.2497	0.1684	-127.977	-8.1797	-1.1021	503.2116	8.1797	1.1021	0	18.180	12.744	-1439.86
7	-0.0128	-0.1532	-127.820	0.0839	1.0029	501.7203	0	0	-360	18.180	12.744	-1799.86
8	0.3035	0.0054	-95.0828	-1.9865	-0.0353	190.7601	0	0	0	18.180	12.744	-1799.86

Table 5: Detailed FRAMBO balancing records. The estimated CR-CG offsets are given in µm, and the slider commands and encoder positions are given in degrees.

Trial	$\hat{x}_{cg}$ [µm]	$\hat{y}_{cg}$ [µm]	$\hat{z}_{cg}$ [µm]	$\Delta s_{\text{raw},x}$ [deg]	$\Delta s_{\text{raw},y}$ [deg]	$\Delta s_{\text{raw},z}$ [deg]	$\Delta s_{\text{cmd},x}$ [deg]	$\Delta s_{\text{cmd},y}$ [deg]	$\Delta s_{\text{cmd},z}$ [deg]	enc_x [deg]	enc_y [deg]	enc_z [deg]
1	0.2316	0.3934	-84.3363	-1.5157	-2.5751	563.6170	0	0	-338.1700	0	0	-338.184
2	0.9817	3.7124	-190.9290	-6.4257	-24.2996	1576.1100	6.4257	24.2996	0	6.408	24.228	-338.184
3	-2.3233	-7.0698	-69.1763	15.2070	46.2752	419.6170	-7.6035	-23.1376	0	-0.972	1.404	-338.184
4	-0.0652	0.4231	-60.2105	0.4268	-2.7693	334.4540	0	0	-200.6724	-0.972	1.404	-538.814
5	0.0958	0.6867	-42.3175	-0.6271	-4.4945	164.4940	0	0	-49.3481	-0.972	1.404	-587.810
6	0.0207	1.2984	-33.3349	-0.1354	-8.4986	79.1702	0	4.2493	0	-0.972	5.328	-587.810
7	-0.1358	0.0075	-36.8673	0.8891	-0.0490	112.7240	0	0	-33.8171	-0.972	5.328	-621.542
8	0.2929	0.3646	-33.6496	-1.9175	-2.3862	82.1594	0	0	-24.6478	-0.972	5.328	-646.094
9	0.6119	0.7235	-30.3074	-4.0053	-4.7358	50.4133	2.0027	2.3679	0	1.116	7.678	-646.094
10	0.0848	0.0938	-23.1258	-0.5551	-0.6139	-17.8027	0	0	0	1.116	7.628	-646.094
11	0.0830	0.1146	-27.6205	-0.5432	-0.7502	24.8911	0	0	0	1.116	7.628	-646.094

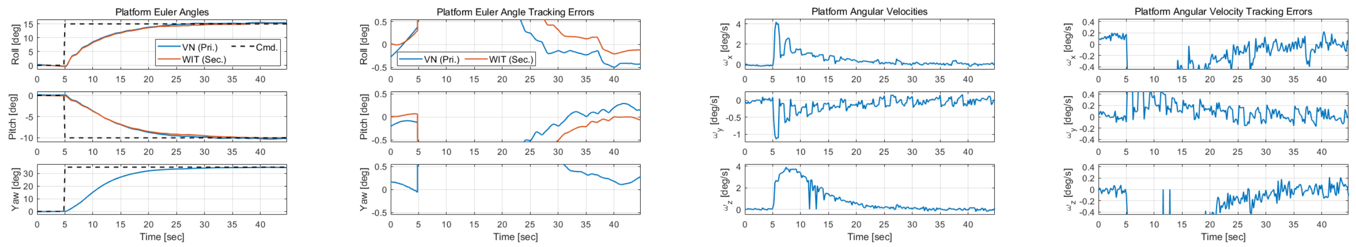

(a) Attitude response. (b) Attitude tracking error. (c) Angular-velocity response. (d) Angular-velocity tracking error.

Figure 5: Three-axis hardware attitude-control results: (**a**) commanded and measured attitude responses; (**b**) attitude tracking errors; (**c**) angular-velocity responses; (**d**) angular-velocity tracking errors.

RAMBO-balanced configuration using the final FRAMBO estimate for gravity-torque feedforward.

4. Discussion

The reported micrometer-level values represent dynamic-equivalent CR-CG offset estimates rather than independent measurements of the physical offset, because sensor errors, unmodeled disturbances, and modeling approximations may be absorbed into the BLS estimate. A slightly negative z_{cg} is intentionally retained for passive restoring stability. Because no PD-only hardware baseline was tested, the independent contribution of the gravity-torque feedforward term cannot be isolated.

The non-orthogonal slider-axis matrix was not explicitly identified, and the stage thresholds and weighting factors were selected empirically for the present hardware; therefore, the observed convergence does not constitute a general convergence guarantee. The implementation is further limited to pre-test/intermittent balancing and relatively low-bandwidth maneuvers because the final FRAMBO estimate is fixed during control and wheel-speed commands are updated at 1.0-s intervals.

5. Conclusions

This study experimentally demonstrated a two-stage automatic mass-balancing and attitude-control framework on a hemispherical 3-DoF spacecraft attitude simulator. CRAMBO completed coarse balancing in eight iterations, followed by eleven FRAMBO trials that refined the dynamic-equivalent CR-CG offset estimate to approximately [0.08, 0.12, −27.62] µm while retaining the required negative vertical offset. The final estimate was used for gravity-torque feedforward in a coupled three-axis hardware maneuver, with attitude errors settling within approximately ±0.5°. These results demonstrate the hardware feasibility of the two-stage balancing procedure and its use in ground-based spacecraft attitude-control testing.

References

[1] J. Prado, G. Bisiacchi, L. Reyes, E. Vicente, F. Contreras, M. Mesinas, A. Juarez, Three-axis air-bearing based platform for small satellite attitude determination and control simulation, Journal of Applied Research and Technology 3 (3) (2005) 222–237. doi:10.22201/icat.16656423.2005.3.03.563.

[2] M. A. Peck, L. Miller, A. R. Cavender, M. Gonzalez, T. Hintz, An airbearing-based testbed for momentum-control systems and spacecraft line of sight, in: 13th Annual AAS/AIAA Space Flight Mechanics Meeting, Vol. 114 of Advances in the Astronautical Sciences, 2003, pp. 427–446, AAS Paper 03-127.

[3] R. C. da Silva, R. A. Borges, S. Battistini, C. Cappelletti, A review of balancing methods for satellite simulators, Acta Astronautica 187 (2021) 537–545. doi:10.1016/j.actaastro.2021.05.037.

[4] R. Boynton, Using a spherical air bearing to simulate weightlessness, in: 55th Annual Conference of the Society of Allied Weight Engineers, 1996, SAWE Paper No. 2297.
URL https://raptor-scientific.com/content/uploads/2020/10/Using_a_Spherical_Air_Bearing_to_Simulate_Weightlessness.pdf

[5] J. J. Kim, B. N. Agrawal, Automatic mass balancing of air-bearing-based three-axis rotational spacecraft simulator, Journal of Guidance, Control, and Dynamics 32 (3) (2009) 1005–1017. doi:10.2514/1.34437.

[6] S. Chesi, Q. Gong, V. Pellegrini, R. Cristi, M. Romano, Automatic mass balancing of a spacecraft three-axis simulator: Analysis and experimentation, Journal of Guidance, Control, and Dynamics 37 (1) (2014) 197–206. doi:10.2514/1.60380.

[7] A. Bahu, D. Modenini, Automatic mass balancing system for a dynamic cubesat attitude simulator: development and experimental validation, CEAS Space Journal 12 (4) (2020) 597–611. doi:10.1007/s12567-020-00309-5.

[8] A. Curatolo, A. Bahu, D. Modenini, Automatic balancing for satellite simulators with mixed mechanical and magnetic actuation, Aerospace 9 (4) (2022) 223. doi:10.3390/aerospace9040223.

[9] Y. Liu, L. Li, Z. Fu, J. Tan, K. Li, Automatic mass balancing of a spacecraft simulator based on non-orthogonal structure, in: 2016 UKACC 11th International Conference on Control (CONTROL), IEEE, Belfast, UK, 2016, pp. 1–6. doi:10.1109/CONTROL.2016.7737579.

[10] G. Di Domenico, F. Topputo, Disturbances quantification for air-bearing spacecraft attitude simulation platforms, in: AIAA SCITECH 2024 Forum, 2024, AIAA Paper 2024-0379. doi:10.2514/6.2024-0379.

[11] D. Thomas, A. T. Wolosik, J. Black, Cubesat attitude control simulator design, in: AIAA Modeling and Simulation Technologies Conference, Kissimmee, Florida, 2018, AIAA Paper 2018-1391. doi:10.2514/6.2018-1391.

[12] Y. Li, Y. Gao, Equations of motion for the automatic balancing system of 3-dof spacecraft attitude control simulator, in: 2010 3rd International Symposium on Systems and Control in Aeronautics and Astronautics, IEEE, Harbin, China, 2010, pp. 248–251. doi:10.1109/ISSCAA.2010.5633650.

[13] B. Wie, H. Weiss, A. Arapostathis, Quaternion feedback regulator for spacecraft eigenaxis rotations, Journal of Guidance, Control, and Dynamics 12 (3) (1989) 375–380. doi:10.2514/3.20418.

[14] B. Wie, Space Vehicle Dynamics and Control, 2nd Edition, American Institute of Aeronautics and Astronautics, Reston, Virginia, 2008. doi:10.2514/4.860119.

[15] D. Jung, P. Tsiotras, An experimental comparison of CMG steering control laws, in: AIAA/AAS Astrodynamics Specialist Conference and Exhibit, Providence, Rhode Island, 2004, AIAA Paper 2004-5294. doi:10.2514/6.2004-5294.